Arab J Geosci (2016) 9:232
DOI 10.1007/s12517-015-2087-x

ORIGINAL PAPER

Tomographic imaging of high seismic activities in underground island longwall face

Anye Cao [1,2] · Linming Dou [1,2] · Wu Cai [2] · Siyuan Gong [2] · Sai Liu [1,2] · Yongliang Zhao [3]

Received: 13 July 2014 / Accepted: 10 September 2015

Abstract Anomalous information identification is a key issue for seismic hazard prevention in underground mining. Velocity tomograms can image the stress redistribution around coal face and provide better understanding of strata failure mechanisms. In this paper, based on microseismic events recorded during mining operation, passive tomographic imagings have been presented to assess strong tremor hazard and locate high seismic activity zones around an island coal face under super-thick strata. The zones of high velocity or velocity gradient anomalies have been found to correlate well with the distribution of strong tremors, indicating that velocity tomography is feasible for seismic hazard assessment and risk region division in underground mining.

Keywords Seismic hazard · Passive tomography · P-wave velocity · Island face · Overburden

✉ Linming Dou
lmdou@cumt.edu.cn

Anye Cao
caoanye@163.com

[1] Key Laboratory of Deep Coal Resource Mining, School of Mines, Ministry of Education of China, China University of Mining and Technology, Xuzhou, Jiangsu 221116, China

[2] State Key Laboratory of Coal Resources and safe Mining, School of Mines, China University of Mining and Technology, Xuzhou 221116, China

[3] Baodian Coal Mine, Yanzhou Coal Mining Company Limited, Zoucheng, Shandong 273513, China

Introduction

Rock bursts and strong tremors are particular cases of seismic events induced by mining activity that results in damage to underground workings or surface buildings. In China, these dynamic hazards are encountered in many coal mines with hard strata, irregular layout, large mining depth, anomaly geological structures, etc. and become progressively more severe (Li et al. 2007; Dou et al. 2012).

Anomalous information identification and analysis is the key issue to reduce and prevent the hazards. Compared to conventional detection methods, e.g., borehole exploration (Qu et al. 2011), pressure sensor installation (Zhang et al. 2014), electromagnetic emission (Wang et al. 2011), acoustic emission (Qi et al. 1994), etc., microseismic monitoring has been proven as a more powerful tool to quantify mining-induced seismicities and can contribute valuable information for mining dynamic hazard control and prevention (Jiang et al. 2006). Meanwhile, as a new geophysical method, the velocity tomography has been gradually used for geologic structure and discontinuity mapping (Peng et al. 2002; Zhao et al. 2000), stress redistribution imaging (Meglis et al. 2005; Mitra and Westman 2009; Friedel et al. 1996; Hosseini et al. 2013; Luo et al. 2009; Luxbacher et al. 2008; Westman et al. 2012), earthquake tomography (Ustaszewski et al. 2012), rock burst detection (Lurka 2008; Banka and Jaworski 2010; Gong 2010), etc. in recent years. Thus, combining the seismic monitoring and velocity tomography imaging may be the new developing direction for seismic hazard assessment or pre-warning in underground mining.

Seismic velocity tomography relies on the transmission of elastic waves through coal-rock mass. Based on the type of source used, tomography can be classified as “active” and “passive” (Luxbacher et al. 2008). Active tomography, which uses controlled explosions, hammer strikes, etc., as the sources, can allow for consistent seismic ray path distribution and is

Published online: 16 March 2016

preferred to apply in the relatively accurate detection of stress distribution and hidden structures in the pre-mining coal faces. For example, Scott et al. conducted active source imaging for pillar tomography in Homestake Mine, USA (Scott et al. 1999). Watanabe et al. used active sources to image coal pillar and triangular area between two drifts (Watanabe and Sassa 1996), while Manthei used active source geometry to image pillars in a potash mine (Manthei 1997). Dou et al. used blasting sources to investigate the relation between wave velocity and high-energy tremors in Jining No. 3 Coal Mine, China (Dou et al. 2012). However, the active detection area does not exceed areas of 200 × 200 m and is not always feasible for long time-lapse investigations (Lurka 2008; Luxbacher et al. 2008).

Passive tomography, which uses mining-induced seismic events as the sources, can continuously estimate the relatively high stress or seismic hazard during the whole mining process, with its detection area up to about 2000 × 2000 m (Lurka 2008). Meanwhile, seismic events in mining areas are frequent enough to allow for ray path density, and more information can be obtained in the rock strata where seismicity occurs. For example, Lurka (2008) used passive sources to assess rock burst hazard and locate high seismic activity zones in Zabrze Bielszowice Coal Mine, Poland. The stress redistribution around a US underground coal longwall panel was studied by passive velocity tomograms (Luxbacher et al. 2008). Meanwhile, passive source imaging was also implemented for pillar tomography in Homestake Gold Mine (Friedel et al. 1996). Passive source studies of tunnels at the Underground Research Laboratory can also be found in the literature (Maxwell and Young 1995; Maxwell and Young 1996). The studies have shown that comprehensive analyses of microseismic activity and computed tomography can provide insight for stress distribution imaging and seismic hazard assessment.

Passive velocity tomography starts fairly late in China and is mostly used in earthquake field (Zhang et al. 2013) and geophysical exploration (Zhao et al. 2000; Peng et al. 2002), while the application in seismic hazard evaluation in underground coal mining has been seldom involved (Gong 2010). The site chosen for this study is an underground island longwall face in Baodian Coal Mine, China, where strong tremors and rock bursts are the main safety threats during mining operation. The island face was monitored by seismic network for 11 months. Thus, the site has considerable microseismic activities, making it ideal for velocity tomographic imaging of high seismic activities during mining process.

Site characteristics

Geological and mining conditions

Strong tremors occurred frequently in Baodian Coal Mine, and the coal production was menaced seriously. The maximal magnitude of seismic tremor is up to 3.7, occurred in LW10304 on May 21, 2005, which caused serious vibration around the whole face. Another, a strong tremor happened in the goafing on Sep. 6, 2004 caused an airproof wall in LW2310 to be destroyed seriously, two people to die, and six people to be injured (Cao 2009).

The main mineable coal beds in Baodian Coal Mine are the Upper and Lower No. 3 Coal Seams, while the average distance between the two seams is about 15 m. LW10302, which mined the Upper No. 3 Coal Seam, is an island longwall face surrounded by three sides of mined areas in No. 10 Mining District. As shown in Fig. 1, LW10301, on the north side of LW10302, has mined both the Upper and Lower No. 3 Coal Seams, while the east half part of LW10303, LW10304, and LW10305 have just mined the Upper No. 3 Coal Seam. Meanwhile, due to coal deposits sterilized under villages, coal seams in west half part of LW10303, LW10304, and LW10305 have not been mined. Moreover, there exit X-F7 and X-F10 faults in the rear of LW10302, while the vertical displacements of the faults are 24 and 14 m, respectively (Cao 2009).

Upper No. 3 Coal Seam, with the average thickness of about 5.8 m, is buried 440~−490 m under the surface. The immediate roof of about 2.68 m in thickness is mainly composed of siltstone, while the main roof is composed of medium sandstone, with the average thickness of 15.85 m. In addition, there exists a primary key stratum (fine sandstone stratum) of nearly 200 m in thickness, approximately 135 m above the Upper No. 3 Coal Seam. During mining process, the super-thick key strata overlying the island and surrounding faces may move together and rupture drastically, which can cause seismic hazards in the vicinity of LW10302. The properties of coal-rock masses can be seen in Table 1.

Fracturing structure of overlying strata

Although both the Upper and Lower No. 3 Coal Seam had been mined out in LW10301, the width of the goafing (about

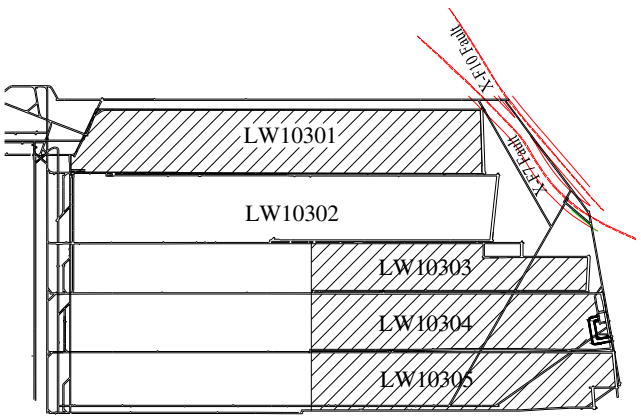

Fig. 1 Layout of LW10302 in No. 10 Mining District

Table 1 Rock properties

Rock strata	Thickness/m	Compressive strength/MPa	Key strata
Topsoil	120		
Fine siltstone	200	70	Primary key strata
Middle strata	34		
Fine sandstone	19.45	70	No. 2 inferior key strata
Middle strata	52		
Medium sandstone	15.85	90	No. 1 inferior key strata
Siltstone	2.68	50	
Upper No. 3 Coal seam	5.80	25	

200 m) is much less than the mining depth (about 450 m) of the coal seam, which means that there was almost no obvious fracturing in the super-thick primary key strata because of the limited mining area. Conversely, the total goafing width of LW10303, LW10304, and LW10305 (about 600 m) is much larger than the mining depth, which means that the overburden above the goafing has caved and ruptured sufficiently. Thus, due to insufficiency mining on the side of LW10301 and sufficiency mining on the side of LW10303, LW10302 is a special unsymmetrical island coal face, while the fracturing structure of primary key strata can be expressed as unsymmetrical T-type structure in the vertical section (Dou et al. 2014). After LW10302 being mined, the overlying key strata above LW10301 and LW10302 may move together; especially the primary "O-X" structures in the plane view will be formed periodically, which will have significant effect on the stress redistribution and occurrence of strong tremors, even rock bursts during mining operation. The simple fracturing structure of overlying strata above LW10302 is shown in Fig. 2.

Passive tomography for strong tremor hazard assessment

Relation between stress and wave velocity

In coal mines, the occurrence of seismic hazards, e.g., rock burst and strong tremor, is closely related to the underground in situ and mining stresses. Velocity tomography is useful for inferring the stress state and stress redistribution in coal-rock mass. Thus, the high seismic activity zones and seismic hazards can be assessed continuously by tomographic imagings. The key of the method relies on the variation of seismic wave (especially P-wave) transmitted through rock mass under stress.

Adams et al. has found that passive tomographic imaging should be built on the close relation between elasticity modulus of rock mass and wave velocity in 1920s (Adams and Williamson 1923). Yale et al. discovered that rock poriness decreases with the increase of stress, which induces the

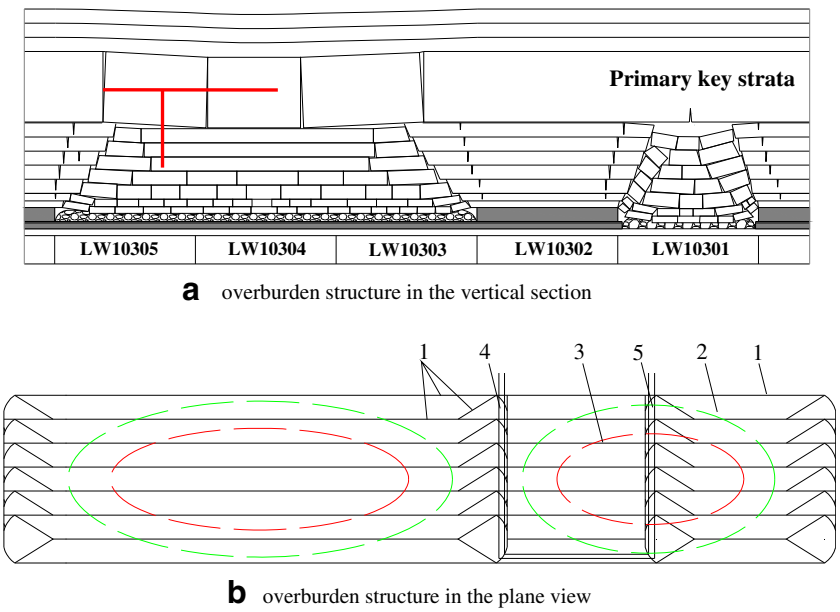

Fig. 2 Sketch of overburden structure above LW10302

increase of wave velocity transmitted in rock mass (Yale 1985). Meanwhile, it is found that obvious change of wave velocity always appears in the high stress stage (Zimmerman and King 1985), and the velocity variation also correlates with the roughness of rock fracture plane (Hopkins et al. 1990). Our existing studies have shown that there is an exponential function relation between ultrasonic wave velocity and axial stress in the uniaxial compression test conditions (Gong 2010), that is, ultrasonic wave velocity usually increases rapidly with the increase of stress at lower stress levels, and after the inelastic phase of rock samples, the increasing extent of wave velocity slows down and gradually turns to be stable at higher stress levels. The typical fitting curves of stress and ultrasonic wave velocity during loading process can be seen in Fig. 3.

Relation between stress and wave velocity in laboratory scale can be extended to the underground mines filed, i.e., high seismic velocity may be expected as the stress increases prior to failure while the low velocity might be expected due to the rock cracks, structure defaults, goafing, etc. The occurrence of seismic hazards, e.g., rock burst and strong tremor, is closely related to underground in situ and mining stresses. Thus, high seismic activity zones and seismic hazards can be assessed by velocity tomographic imagings.

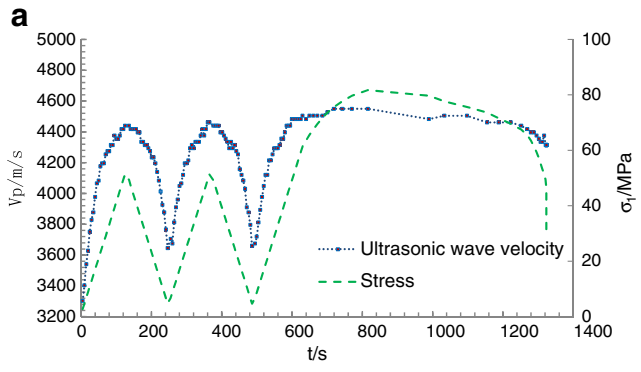

Variation laws of wave velocity and stress associated with loading time

Relation between wave velocity and stress under uniaxial loading

Fig. 3 Relationship between stress and ultrasonic wave velocity under uniaxial compression loading

Theory of passive velocity tomography

The idea of seismic tomography was originated from the use of X-ray computed tomography (CT) in medicine, which is able to determine uniquely any abnormal absorption tissue in a cross section of the body of a patient (Radon 1917). It requires dividing the body into grid cells called pixels in two-dimensional situation or cubes called voxels in three-dimensional situation to estimate the body characteristics in all pixels or voxels (Cai et al. 2014). Based on the same key principles, tomography was extended to the geophysical field by using seismic waves, which is known as seismic tomography. According to the inversion parameters of seismic wave, seismic tomography can be classified as velocity tomography and attenuation tomography (Westman et al. 1996). In velocity tomography, the parameter is the inversion of velocity distribution with travel time, and attenuation tomography focuses on measuring the amplitude of seismic waves to detect the absorption property of geological media. In addition, seismic velocity tomography based on the type of source used is classified as active and passive (Gibowicz and Kijko 1994; Luxbacher et al. 2008).

In passive tomography, the mining-induced seismic events are utilized as sources, which can be illustrated in Fig. 4. Seismic events in mining areas are frequent enough to allow for ray path density, and more information can be obtained in rock strata where seismicity occurs. Compared to active tomography, passive velocity tomography can estimate the relatively high stress zone continuously during the whole mining process, and its detection area is larger. Also, the inversion accuracy of passive tomography may be affected duo to the location error of seismic source. However, the seismic activities mainly locate around the current mining area; especially the layout density of seismic monitoring network in stress concentration area is relatively high, which can provide adequate spatial ray coverage of the mining area and improve the reliability of velocity inversion results (Fig. 5).

Velocity tomography depends on the relation that the wave velocity along a seismic ray is the ray path distance divided by the time to travel between the seismic source and receiver. Suppose the ray path of the ith seismic wave is L_i and the travel time is T_i, thus, the time is the integral of

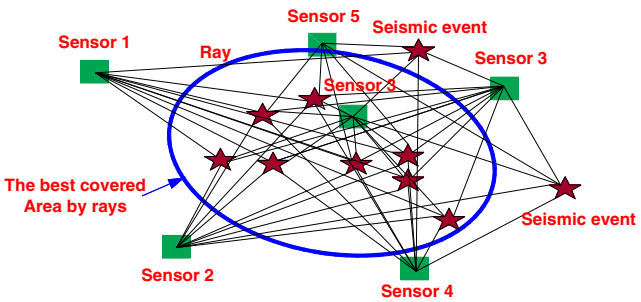

Fig. 4 Illustration of passive velocity tomography

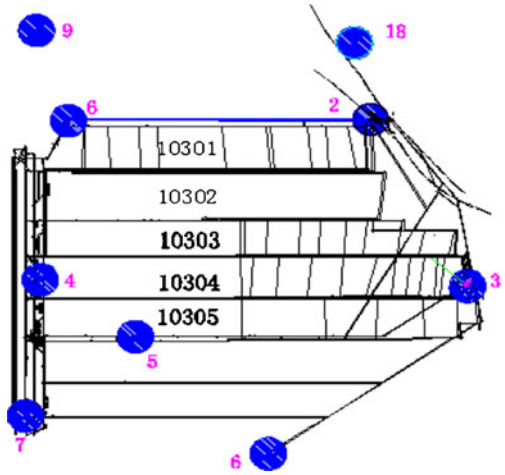

Fig. 5 Layout of sensor stations around District 10

the inverse velocity, $1/V(x,y,z)$, or slowness, $S(x,y,z)$, from the seismic source to the receiver, as shown in Eq. (1)~Eq. (2) (Gibowicz and Kijko 1994; Luxbacher et al. 2008):

$$V = \frac{L}{T} \rightarrow VT = L \tag{1}$$

$$T_i = \int_{L_i} \frac{dL}{V(x,y,z)} = \int_{L_i} S(x,y,z)dL \tag{2}$$

where $V(x,y,z)$ is the velocity (m/s), L is the distance (m), T is the travel time (s), and $S(x,y,z)$ is the slowness (s/m).

It is known that $V(x,y,z)$ and L_i are variables, so this equation is nonlinear. If little change occurs for the velocity structure, the ray path L_i can be treated as a straight line; however, the path is usually a curve in fact due to the complexity of rock mass; we need discrete inversion area to m grids. So, the travel time of the ith ray can be presented as Eq. (3):

$$T_i = \sum_{j=1}^{m} d_{ij} S_j \quad (i = 1, \cdots, n) \tag{3}$$

where d_{ij} is the distance of the ith ray crossing the jth voxel, n is the total number of rays, and m is the number of voxels.

When massive seismic ray paths pass through the inversion region, arranging the travel time, distance, and slowness for each voxel into matrices, the velocity can be determined through inverse theory as shown in Eq. (4):

$$\begin{cases} T_1 = d_{11}S_1 + d_{12}S_2 + d_{13}S_3 + \cdots + d_{1j}S_j \\ T_2 = d_{21}S_1 + d_{22}S_2 + d_{23}S_3 + \cdots + d_{2j}S_j \\ \cdots \quad \cdots \\ T_i = d_{i1}S_1 + d_{i2}S_2 + d_{i3}S_3 + \cdots + d_{ij}S_j \end{cases} \tag{4}$$

Generally, microseismic event location and subsequent rays are calculated using an initial velocity model. However, the velocity, distance, and time in an individual voxel are not known. Arranging the time, distance, and slowness for each voxel into matrices, the velocity can be determined through inverse theory as follows (Luxbacher et al. 2008):

$$\mathbf{T} = \mathbf{DS} \rightarrow \mathbf{S} = \mathbf{D}^{-1}\mathbf{T} \tag{5}$$

where $\mathbf{T}$ is the column vector of travel times ($n \times 1$), $\mathbf{D}$ is the matrix of ray distances ($n \times m$), and $\mathbf{S}$ is the column vector of slowness values ($m \times 1$).

The matrix inversion methods are effective but require considerable computational power for large datasets. Usually, the inverse problem is either underdetermined (more voxels than rays) or overdetermined (more rays than voxels) (Luxbacher et al. 2008; Cai et al. 2014). The most effective way to solve this problem is iterative process. Currently, the most referenced iterative methods are algebraic reconstructive technique (ART) and simultaneous iterative reconstructive technique (SIRT) (Gilbert 1972).

SIRT is an appropriate algorithm and was adopted in this paper. In the solving process, seismic event locations were recalculated and the slowness in each cell with regards to all the passing rays was modified once per cycle. Above steps were repeated until the residual time was less than an acceptable amount or the number of iterative reached the threshold value.

Assessment model of seismic hazard by passive velocity tomography

In underground mining, there may exit positive anomaly of P-wave velocity in high stress or stress concentration region. Positive velocity anomaly is expressed in Eq. (6) (Gong 2010; Gibowicz and Kijko 1994):

$$A_n = \frac{V_p - V_p{}^a}{V_p{}^a} \tag{6}$$

where V_P is P-wave velocity of a certain point and $V_p{}^a$ is the average velocity of the model.

The relation between positive anomaly of wave velocity and stress concentration degree can be shown in Table 2.

Meanwhile, seismic hazards are also liable to occur along the zones with obvious velocity gradients. VG value is used to express the variation degree of velocity

Table 2 Relation between positive anomalies of wave speed and stress concentration

Seismic risk index	Stress concentration degree	Positive velocity anomaly A_n, %
0	None	<5
1	Weak	5~15
2	Middle	15~25
3	Strong	>25

gradient, and the anomaly of VG can be shown in Eq. (7) (Gong 2010):

$$A_n = \frac{VG - VG^a}{VG^a} \tag{7}$$

where VG^a is the average value of the model.

Similarly, the relation between VG anomaly of wave velocity and seismic hazard degree can be shown in Table 3.

Case study

Inversion parameters

SOS microseismic monitoring system, which was introduced from Poland, has been installed in Baodian Coal Mine. Figure 5 displays the plane view of longwall geometry and sensor locations over No. 10 Mining District; there are nine sensors (blue circles) used to monitor the seismicities around No. 10 Mining District. The layout of sensor stations was optimized by numerical experiment of D-optimal design, and the expected average location error is less than 20 m around No. 10 Mining District (Gong 2010), which can provide accurate initial locations for passive velocity inversions, and ensures enough coverage density of ray paths. The data acquisition for passive tomographic imagings during LW10302 mining were conducted with the seismic monitoring system, which utilizes seismic events as the energy sources and measures P-wave arrival times after seismic waves pass through coal-rock mass. After data reduction, the data were analyzed using MINESOSTOMO program developed by Gong (2010).

Table 3 Relation between VG anomaly and seismic hazard

Seismic risk index	Seismic risk degree	VG anomaly A_n, %
0	None	<5
1	Weak	5–15
2	Middle	15–25
3	Strong	>25

To decrease the grid model size, improve the inversion efficiency, and avoid the inconsistent spatial distribution, the passive velocity tomography on LW10302 was performed using the stations (#2, #3, #4, #5, #6, #7, #8, #9, and #18) and the seismic events located in the target areas. Moreover, the seismic events recorded by over five stations were adopted to avoid creating artificial anomaly in tomograms. Calculations have been made in 11-month time intervals from July, 2009 to May, 2010. Because the layout density of monitoring network around No. 10 Mining District is relatively high and the seismic activities were quite active during the mining process, the network can provide adequate spatial seismic ray coverage of the entire area of study.

Actually, tomographic imaging mainly depends on velocity distribution, source-receiver geometry and density, variable gridding, etc. The inversion iteration of tomograms in this study was conducted using SIRT which must have an initial velocity value to perturb the first iteration. The initial velocity model allows the inversion and source locations to be more efficient and accurate. The source-receiver geometry and density will also affect the source location accuracy and determine how well the ray coverage will be. The variable gridding determines the resolution of seismic tomography, i.e., allows areas that are not well sampled to be adequately constrained.

Considering that the strike (in X direction) and inclined (in Y direction) lengths of No. 10 Mining District are 2 and 1.5 km, respectively, and the mining depth (in Z direction) of the Upper No. 3 Coal Seam is about 450 m, to ensure that the seismic ray density can satisfy inversion requirement and improve the computational efficiency, total $71 \times 61 \times 5$ voxel points, with each voxel size of $30 \times 30 \times 125$ m in X, Y, and Z directions, respectively, was input into for tomographic calculation. A layer initial P-wave velocity model in calculation was assumed in the investigation area, based on geophysical data that has been previously collected, while the constant P-wave velocity equal to 4.5 km/s was assumed to calculate the seismic event location and perturb the first iteration. To reduce the indeterminacy, the velocity was limited in constant gradient between 2.0~6.5 km/s from top to bottom. Additionally, the ray tracing method used for velocity calculation is the hybrid algorithm combined with shortest path method and ray bending method, while the inversion iteration was conducted by SIRT.

Tomography practice in LW10302

In this paper, plane view velocity tomograms at seam level, $z = -400$ m, were generated for each month, to evaluate the areas and degrees of high seismic hazards in the next mining period.

1. July 15 to July 31, 2009

   Mining operation in LW10302 was started on July 15, 2009 and completed on May 31, 2010. The face was retreated about 45 m at the end of July. In this period, over

542 events associated with roof and floor breakages were recorded, while 102 seismic events were selected for passive tomographic imaging because each of them were recorded and located by over five geophone stations. Calculated velocity image and velocity gradient anomaly image are shown in Fig. 6. High velocity and velocity gradient anomaly can be observed near the open-off cut of LW10301 and the coal pillar region of faults X-F7 and X-F10, and the maximal value of P-wave velocity is up to 6118 m/s, while the maximum positive anomalies of velocity is 0.36, which indicates that the areas mentioned above were at a strong seismic hazard risk at present stage and in further mining period due to the large-scale overburden above LW10301 may move or fault structures may be reacted by mining disturbance.

Four strong tremors with seismic energy over 10^5 J were recorded between Aug. 1 and Aug. 31. As shown in Fig. 6, the strong tremors were located well in the

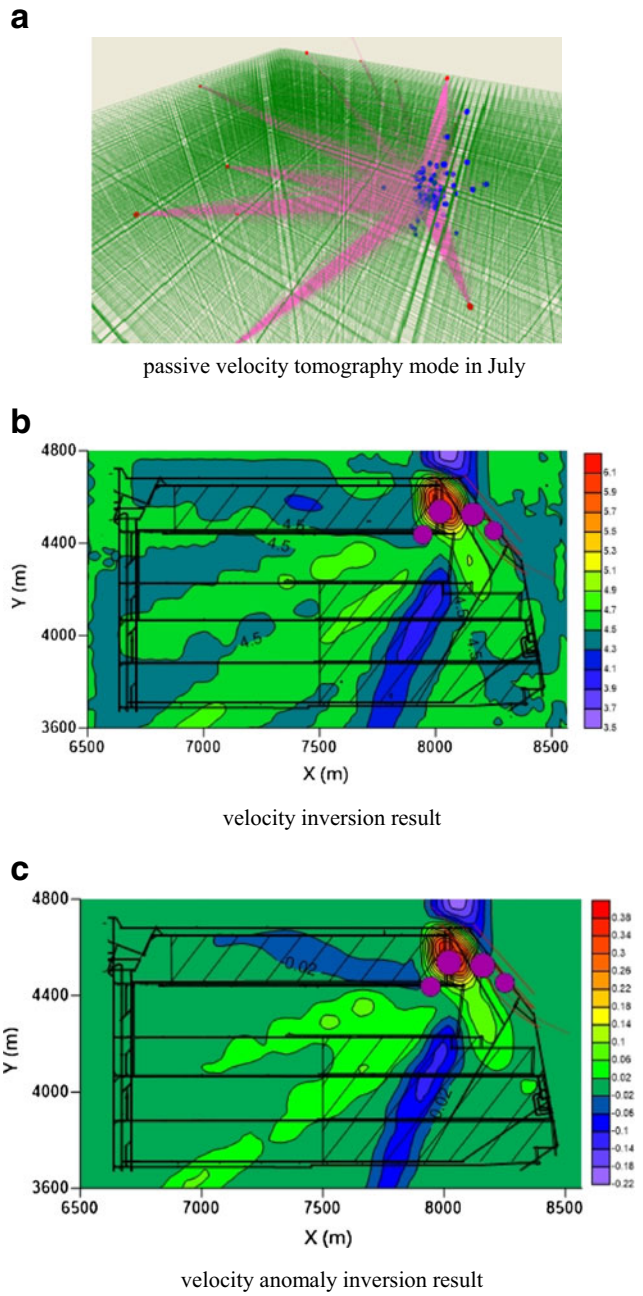

Fig. 6 Tomography images obtained using seismic events between July 15 and July 31 (in **a**, *green line* means the constructed model, *red points* are sensors, *blue points* are seismic sources, *pink lines* are ray paths, while *circle symbols* in **b** and **c** show positions of strong tremors with energies $E > 10^5$ J that occurred between Aug. 1 and Aug. 31)

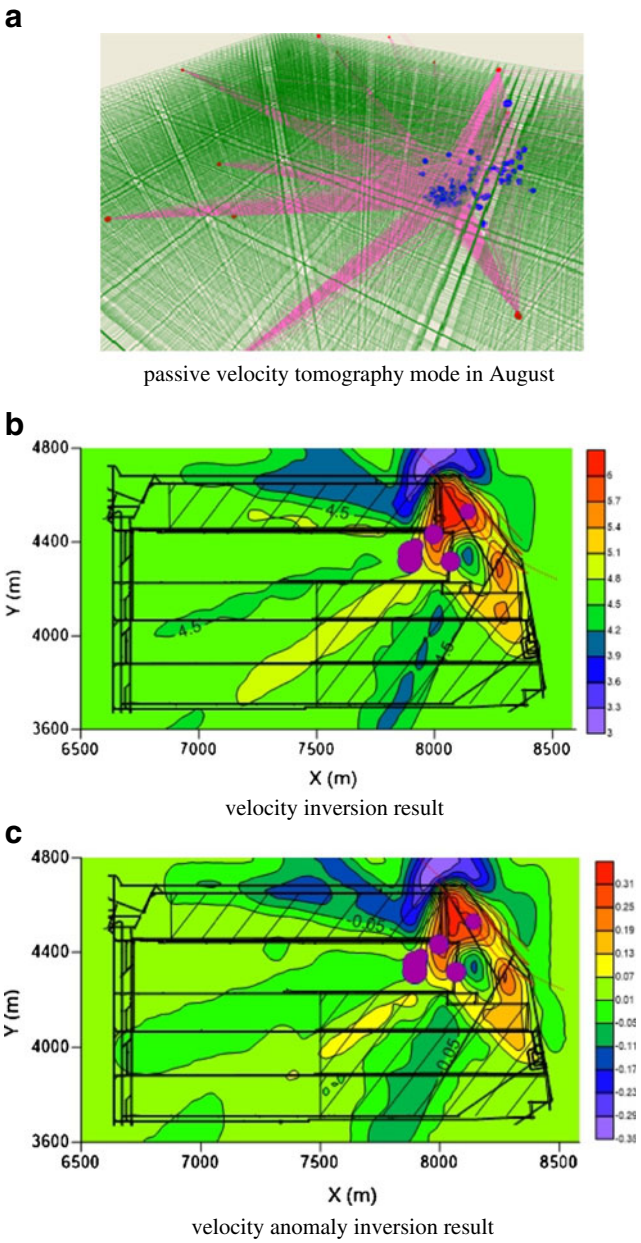

Fig. 7 Tomography images obtained using seismic events between Aug. 1 and Aug. 31 (*circle symbols* show positions of strong tremors with energies $E > 10^5$ J that occurred between Sep. 1 and Sep. 30)

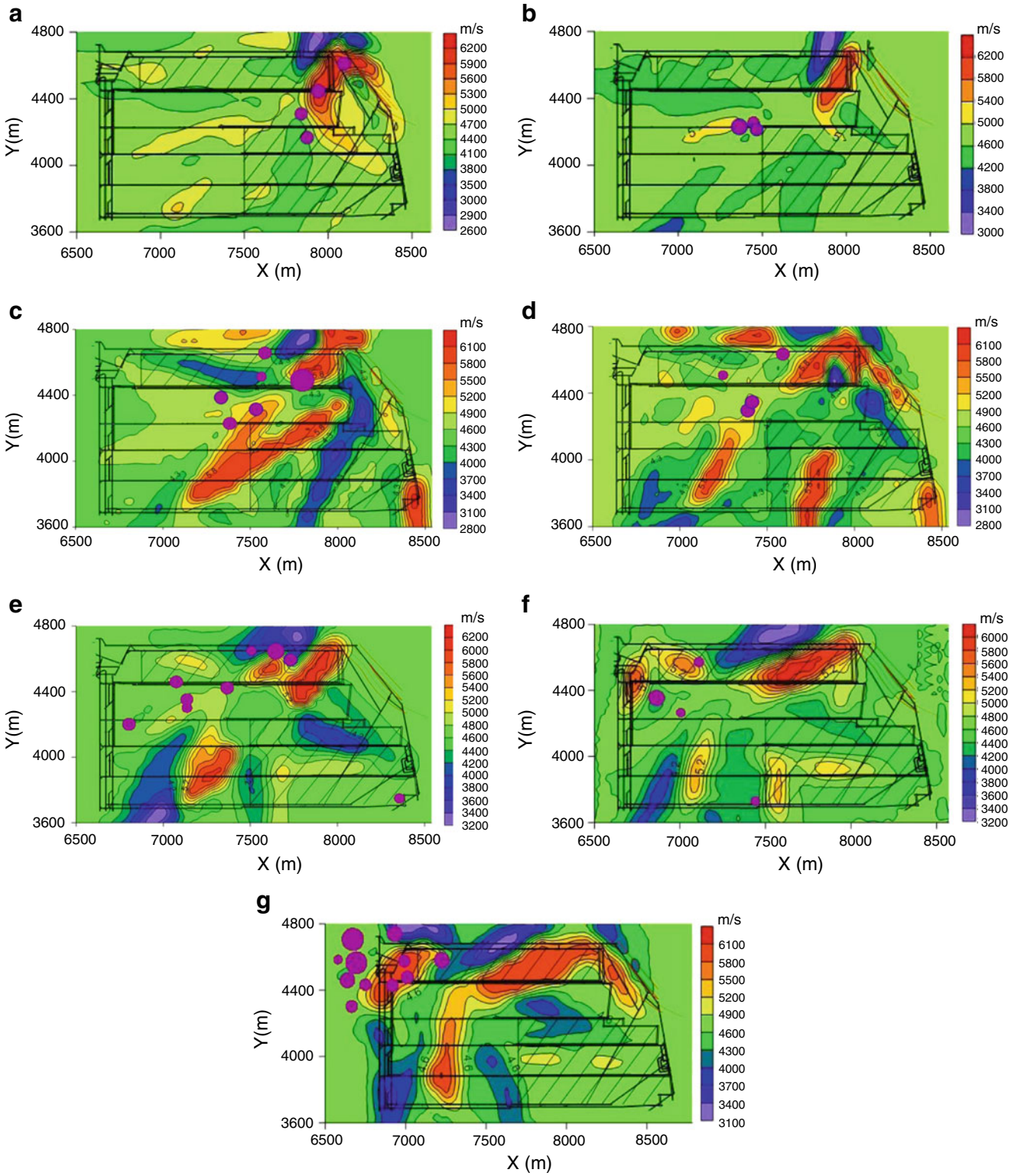

Fig. 8 Tomography images in each month during the period from Sep. 1, 2009 to Mar. 31, 2010 (*circle symbols* show positions of strong tremors with energies $E > 10^5$ J that occurred in the next period of the corresponding velocity inversion)

vicinity of high-velocity area and the area of high-velocity gradient. Almost all the strong tremors caused underground strata behaviors and surface transitory shakings at different degrees. The results show that the strong tremors correlate well with the high-velocity zones and high-velocity gradient zones.

2. Aug. 1 to Aug. 31, 2009

   LW10302 was retreated about 85 m in Augest, which means that the mining intensity was somewhat increased comparing with the initial mining period. Calculated velocity images are shown in Fig. 7. In this period, high velocity or velocity anomaly zone increases and starts to move toward LW10302 direction, which indicates that large-scale overburden above LW10301 and LW10302 may move together. Six strong tremors with seismic energy over 10^5 J were recorded between Sep. 1 and Sep. 30. As shown in Fig. 7, most of the strong tremors were located within the high-velocity area and the area of high-velocity gradient.

3. Sep. 1, 2009 to Mar. 31, 2010

   Tomographic velocity images in Fig. 8 show further changes of P-wave velocity during the mining period of LW10302 from Sep. 1, 2009 to Mar. 31, 2010. The high-velocity regions were observed to redistribute as LW10302 retreated, from the goafing area of LW10301 to the area ahead of LW10302, and to the protective pillar area of No. 10 Mining District. Moreover, most of the future strong tremors with energy over 10^5 J occurred above LW10301 and LW10302, within or near to the relatively high-velocity zones.

4. Apr. 1, to Apr. 30, 2010

   Calculated velocity image is shown in Fig. 9. As LW10302 retreated gradually toward the terminal line, high velocity and velocity gradient anomaly regions were observed to concentrate near the protective pillar area of No. 10 Mining District and the goafing areas above LW10301 and 10302, which indicates that there exits large-scale strata movement above the goafing and causes high stress concentration in the protective coal pillar with the constant increase of mined-out areas in LW10302. Five strong tremors with energy over 10^5 J were recorded between May 1 and May 31, 2010. As shown in Fig. 7, nearly all the strong tremors occurred near the protective pillar area and correlated well with the high velocity and velocity anomaly areas.

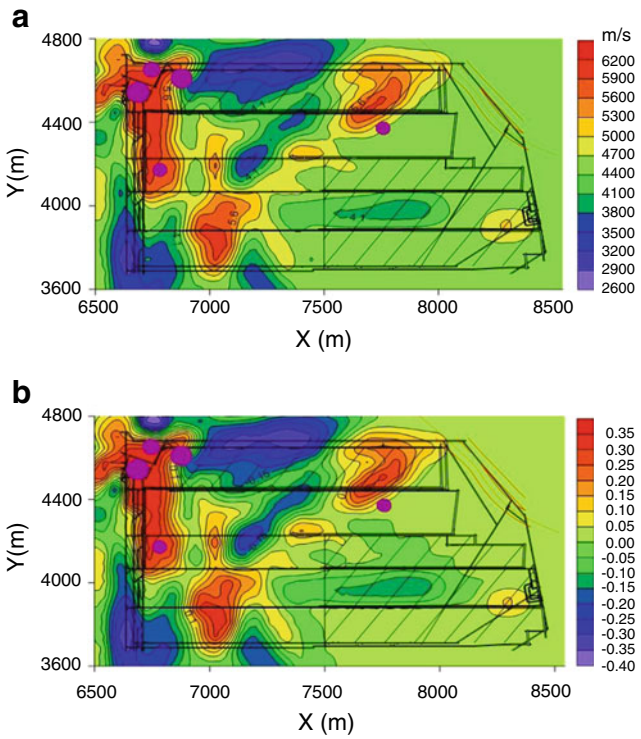

Fig. 9 Tomography images obtained using seismic events between Apr. 1 and Apr. 30, 2010 (*circle symbols* show positions of strong tremors with energies $E > 10^5$ J that occurred between May 1 and May 31, 2010)

Conclusions

In this paper, a new method for seismic hazard assessment and pre-warning in underground mining was developed through combining seismic monitoring and tomography imaging. An island coal face under super-thick strata, LW10302, which may suffer from the threats of strong tremors, was chosen for velocity tomography study. The results from LW10302 confirm a good correlation between the areas of high velocity or velocity anomalies and the areas of high seismic activities. Through the tomography detection practice, this technique is feasible for dynamic hazard assessment and risk region division. The development of passive tomographic imaging can improve the seismic monitoring and pre-warning level for strong tremors or rock bursts in coal mines.

In the future, passive velocity tomography coupled with the active tomography, as well as some traditional detection methods, will assist in obtaining more accurate results and contribute to a safer and more productive environment in underground mining.

Acknowledgments This research is supported by National Natural Science Foundation of China (51204165), National Twelfth Five-Year Key Science and Technology Foundation of China (2012BAK04B06), Fundamental Research Funds for the Central Universities (2014XT01, 2012BZB17), and Project of PADD funded by the Priority Academic Program Development of Jiangsu Higher Education Instruction (SZBF2011-6-B35).

References

Adams L, Williamson E (1923) On the compressibility of minerals and rocks at high pressures. J Franklin Inst 195:475–531

Banka P, Jaworski A (2010) Possibility of more precise analytical prediction of rock mass energy changes with the use of passive seismic tomography readings. Arch Min Sci 55:723–731

Cai W, Dou LM, Cao AY, Gong SY, Li ZL (2014) Application of seismic velocity tomography in underground coal mines: a case study of Yima mining area, Henan, China. J Appl Geophys 109(10):140–149

Cao AY (2009) Research on seismic effort of burst and failure of coal-rock mass associated with mining and its application. China University of Mining and Technology, Xuzhou

Dou LM, Chen TJ, Gong SY, He H, Zhang SB (2012) Rockburst hazard determination by using computed tomography technology in deep workface. Saf Sci 50(4):736–740

Dou LM, He XQ, He H, He J, Fan J (2014) Spatial structure evolution of overlying strata and inducing mechanism of rockburst in coal mine. Trans Nonferrous Metals Soc China 24(4):1255–1261

Friedel MJ, Scott DF, Jackson MJ, Williams TJ, Killen SM (1996) 3-D tomographic imaging of anomalous stress conditions in a deep US gold mine. J Appl Geophys 36(1):1–17

Gibowicz SJ, Kijko A (1994) An introduction to mining seismology. Academic Press, San Diego

Gilbert P (1972) Iterative methods for the three-dimensional reconstruction of an object from projections. J Theor Biol 36:105–117

Gong SY (2010) Research and application of using mine tremor velocity tomography to forecast rockburst danger in coal mine. China University of Mining and Technology, Xuzhou

Hopkins DL, Cook NGW, Myer LR (1990) Normal joint stiffness as a function of spatial geometry and surface roughness. In: Barton N, Stephansson O (eds) Rock Joints. Balkema, Rotterdam, pp 203–210

Hosseini N, Oraee K, Shahriar K, Goshtasbi K (2013) Studying the stress redistribution around the longwall mining panel using passive seismic velocity tomography and geostatistical estimation. Arab J Geosci 6:1407–1416

Jiang FX, Yang SH, Cheng YH, Zhang XM, Mao ZY, Xu FJ (2006) A study on microseismic monitoring of rock burst in coal mine. Chinese Journal Geophysics 49(5):1511–1516

Li T, Cai MF, Cai M (2007) A review of mining-induced seismicity in China. International Journal of Rock Mechanics & Mining Sciences 44:1149–1171

Luo X, King A, Van de Werken M (2009) Tomographic imaging of rock conditions ahead of mining using the shearer as a seismic source—a feasibility study. IEEE Trans. Geosci. Remote Sens 47:3671–3678

Lurka A (2008) Location of high seismic activity zones and seismic hazard assessment in Zabrze Bielszowice coal mine using passive tomography. China University Mining & Technology 18:177–181

Luxbacher K, Westman E, Swanson P, Karfakis M (2008) Three-dimensional time-lapse velocity tomography of an underground longwall panel. International Journal of Rock Mechanics and Mining Sciences 45(4):478–485

Manthei G (1997) Seismic tomography on a pillar in a potash mine. In: Proceedings of the 4th international symposium rockbursts and seismicity in mines, Krakow: 237–242.

Maxwell SC, Young RP (1995) A controlled in-situ investigation of the relationship between stress, velocity and induced seismicity. Geophys Res Lett 22:1049–1052

Maxwell SC, Young RP (1996) Seismic imaging of rock mass responses to excavation. Int J Rock Mech Min Sci Geomech Abstr 33: 713–724

Meglis I, Chow T, Martin C, Young R (2005) Assessing in situ microcrack damage using ultrasonic velocity tomography. Int J Rock Mech Min Sci 42:25–34

Mitra R, Westman E (2009) Investigation of the stress imaging in rock samples using numerical modeling and laboratory tomography. Int J Geotech Eng 3:517–525

Peng SP, Ling BC, Liu SD (2002) Application of seismic tomography in longwall top-coal caving face. Chin J Rock Mech Eng 21(12):1786–1790

Qi QX, Li SB, Wang SK (1994) Application of AE technique in monitoring ground pressure. Journal of China Coal Society 19(3):221–232

Qu XC, Jiang FX, Yu ZX (2011) Rockburst monitoring and precaution technology based on equivalent drilling research and its application. Chin J Rock Mech Eng 30(11):2346–2351

Radon J (1917) Über die bestimmung von funktionen durch ihre integralwerte lange gewisser mannigfaltigkeiten. Ber Verh Saechs Akad Wiss 69:262–267

Scott D F, Girard J M, Williams T J, Denton D K (1999) Comparison of seismic tomography, strain relief, and ultrasonic velocity measurements to evaluate stress in an underground pillar. In: Proceedings of society for mining metallurgy and exploration annual meeting, Denver.

Ustaszewski K, Wu Y-M, Suppe J, Huang HH, Chang CH, Carena S (2012) Crust-mantle boundaries in the Taiwan-Luzon arc-continent collision system determined from local earthquake tomography and 1D models: implications for the mode of subduction polarity reversal. Tectonophysics 578:31–49

Wang EY, He XQ, Wei JP, Nie BS, Song DZ (2011) Electromagnetic emission graded warning model and its applications against coal rock dynamic collapses. Int J Rock Mech Min Sci 48:556–564

Watanabe T, Sassa K (1996) Seismic attenuation tomography and its application to rock mass evaluation. Int J Rock Mech Min Sci 33: 467–477

Westman EC, Haramy KY, Rock AD (1996) Seismic tomography for longwall stress analysis. Rock Mechanics Tools and Techniques. Aubertin, Hassani & Mitri, pp 397–403

Westman E, Luxbacher K, Schafrik S (2012) Passive seismic tomography for three-dimensional time-lapse imaging of mining-induced rock mass changes. Lead Edge 31:338–345

Yale D (1985) Recent advances in rock physics. Geophysics 50(12): 2480–2491

Zhang FX, Wu QJ, Li YH (2013) The traveltime tomography study by teleseismic P wave data in the Northeast China area. Chin J Geophys–Chinese Ed 56:2690–2700

Zhang N, Zhang NC, Han CL, Qian DY, Xue F (2014) Borehole stress monitoring analysis on advanced abutment pressure induced by longwall mining. Arab J Geosci 7:457–463

Zhao YG, Li Q, Guo H, Jin HX, Wang CF (2000) Seismic attenuation tomography in frequency domain and its application to engineering. Science in China (Series D) 43(4):431–438

Zimmerman R W, King M S (1985) Propag/ation of acoustic waves through a cracked rock. Proc. 26th U.S. Symposium on Rock Mechanics, Rapid City: 739–745.